Australian Government
Department of Defence
Science and Technology

Bubble Cloud Generation by an Airgun: Laboratory Experiments and Modelling

Alexei Kouzoubov and Shane Wood

Maritime Division
Defence Science and Technology Group

DST-Group-TR-3379

ABSTRACT

Laboratory experiments in support of the development and validation of a model of bubble cloud resulting from an underwater explosion are described in this report. The underwater explosion was emulated by a small airgun. The elements of the model are presented in detail. Special attention is paid to the model improvements with respect to accounting for bubble interaction in the rising bubble cloud through water entrainment. Model results are compared to the experimental measurements and high-fidelity numerical simulations.

Produced by

Maritime Division
Defence Science and Technology Group
PO Box 1500
Edinburgh SA 5111

Telephone: 1300 333 362

July 2017
AR-016-902

APPROVED FOR PUBLIC RELEASE

Bubble Cloud Generation by an Airgun: Laboratory Experiments and Modelling

Executive Summary

The Defence Science and Technology Group collaborates with the United States Naval Undersea Warfare Center (NUWC) in the development of various bubbly wake models for the Weapons Analysis Facility (WAF), and its Australian version, the Torpedo Analysis Facility (TAF). There is a requirement under the WAF/TAF model development program to develop a model of a bubble cloud generated by an underwater explosion (UNDEX). The ultimate purpose of such a model is to simulate the response of the bubble cloud to an active sonar pulse. For this, the size distribution of the bubbles resulting from the disintegration of the initial explosion bubble needs to be known. The bubble size distribution in the UNDEX remnant bubble cloud is not static and changes with time mainly due to the rise of bubbles to the surface, but also bubble coalescence and break-up. The problem of the rising bubble cloud is mathematically simpler to model than the problem of the explosion bubble disintegration into smaller bubbles, but is still too complex to solve analytically. The complexity of the multiphase flow in the rising bubble cloud is caused by the presence of bubbles of many different sizes and their interaction with each other, mainly through the water entrained by the bubble motion.

A previously developed model of the remnant bubble cloud of an underwater explosion did not take into account the motion of entrained water and its influence on the bubble rise. In this research the model has been improved by taking into account interaction between bubbles through water entrainment. In the new model the bubbles in the cloud are divided into two fractions of large and small bubbles, and a simplified model of water entrainment by the large bubble fraction has been developed. The dynamics of the rising small bubbles is calculated on the assumption that their velocity is constant and is the sum of the terminal velocity in still water and that of the entrained water. The time history of the bubble size and spatial distribution in the cloud can then be easily computed. The calculation of acoustic properties of the bubble cloud is straightforward after that.

To validate the new model, an experiment was conducted in the acoustic tank of the Underwater Acoustic Scattering Laboratory. The underwater explosion was emulated by a small airgun. The model of the explosion bubble dynamics was modified to the parameters of the airgun. The modified model is demonstrating a fair agreement with measured time history of the oscillating bubble radius. The simplified model of the water entrainment was validated by comparison of the water velocity at the axis of the bubble cloud with the corresponding measurements using an acoustic Doppler velocimeter. Finally, a comparison was made between the simulated and measured acoustic transmission through the bubble cloud. Although a perfect agreement was not achieved, a significant improvement compared to the previous model was demonstrated.

This page is intentionally blank.

Authors

Alexei Kouzoubov
Maritime Division

Alexei Kouzoubov is a Senior Research Scientist in the Maritime Operations Division at Defence Science and Technology (DST) Group, Edinburgh. He has a PhD in Computational Fluid Dynamics from the Institute for High Temperatures of the Russian Academy of Sciences. He has previously worked at the Universities of Adelaide, New South Wales, and South Australia before joining DST Group in 1998. His research interests include active sonar classification, acoustic modelling and fluid dynamics of multiphase flows.

Shane A. Wood
Maritime Division

Shane Wood joined Defence Science and Technology Group in 1986 as an apprentice Precision Optical Mechanic. He has completed Diplomas in Electronic, Computer Systems, and Mechanical Engineering. Shane has worked in the areas of data analysis, data acquisitions, and sea trials. He is currently involved in the development, maintenance, and operation of the Underwater Acoustic Scattering Laboratory at Maritime Division, Edinburgh.

This page is intentionally blank.

Contents

This page is intentionally blank.

1. Introduction

The Defence Science and Technology (DST) Group is collaborating with the United States Naval Undersea Warfare Center (NUWC) in the development of various bubbly wake models for the Weapons Analysis Facility (WAF) and its Australian version, the Torpedo Analysis Facility (TAF). There is a requirement under the WAF/TAF model development program to develop a model of a bubble cloud generated by an underwater explosion (UNDEX). The ultimate purpose of such a model is to simulate the response of the bubble cloud to an active sonar pulse. For this, the size distribution of the bubbles resulting from the disintegration of the initial explosion bubble needs to be known. The bubble size distribution in the UNDEX remnant bubble cloud is not static and changes with time mainly due to the rise of bubbles to the surface, but also bubble coalescence and break-up. The problem of the rising bubble cloud is mathematically simpler to model than the problem of the explosion bubble disintegration into smaller bubbles, but is still too complex to solve analytically. The complexity of the multiphase flow in the rising bubble cloud is caused by the presence of bubbles of many different sizes and their interaction with each other, mainly through the water entrained by the bubble motion.

A previously developed model [1] did not take into account the motion of entrained water and its influence on bubble rise. However, it was clear from the previous tank experiments where the bubble cloud was generated by a canister with compressed air [2] that the measured time history of the acoustic response of the rising bubble cloud disagrees significantly with the model. This was explained by the interaction of the larger and smaller bubbles in the bubble cloud through entrainment of water. The water entrained by the larger bubbles made the smaller bubbles rise quicker. It is not simple to calculate the velocity of entrained water analytically even if the bubble size distribution in the cloud is known. The Computational Fluid Dynamics (CFD) simulations of water entrainment by the rising bubble cloud are possible but with a limited number of bubble size fractions. For a computationally efficient model desirable for WAF/TAF implementation it is important to develop a sufficiently accurate approximate analytical model of the rising bubble cloud. Both experiments and high fidelity CFD simulations can help in the development and validation of such a model.

Previous laboratory experiments [2] did not include the measurements of the velocity of water in the rising bubble cloud. The experiments reported in the current document do include such measurements. They were also conducted with a different bubble cloud source. The previous experiments with a compressed air canister did not provide a sufficiently accurate emulation of an underwater explosion. This was due to relatively low pressure in the canister and the slow opening of the valve used for air release. In the latest experiments a small airgun was used which emulated the explosion bubble better than the bubble generated by the compressed air canister.

2. Experiments

Experiments were conducted in the water tank of the Underwater Acoustic Scattering Laboratory (UASL). The following data were collected during the experiments: high-speed videos of the initial bubble, still images of the rising bubble cloud, velocity of water in the rising bubble cloud, acoustic scattering from and transmission through the bubble cloud.

2.1 Experiment Set-up

The experiment set-up is illustrated in Figure 1. The charged airgun was placed in the tank at a depth of 2 metres. Different types of data were collected in separate experiments; in other words, in every individual run only one type of data was obtained. High-speed videos and still images of the initial airgun bubble and the rising bubble cloud were obtained through a glass window in the tank wall. The velocity of water in the rising bubble was measured using the Nortek Vectrino profiler with the sampling volume placed on the axis of the rising bubble cloud at 0.5 metres above the airgun. The acoustic scattering from the bubble cloud and acoustic transmission through it were obtained using the ITC transducer with the centre frequency of 100 kHz. The transducer was positioned with its beam axis crossing the bubble cloud at 0.5 metres above the airgun. A hydrophone was placed on the beam axis of the transducer on the opposite side from the bubble cloud to measure the acoustic transmission through bubbles.

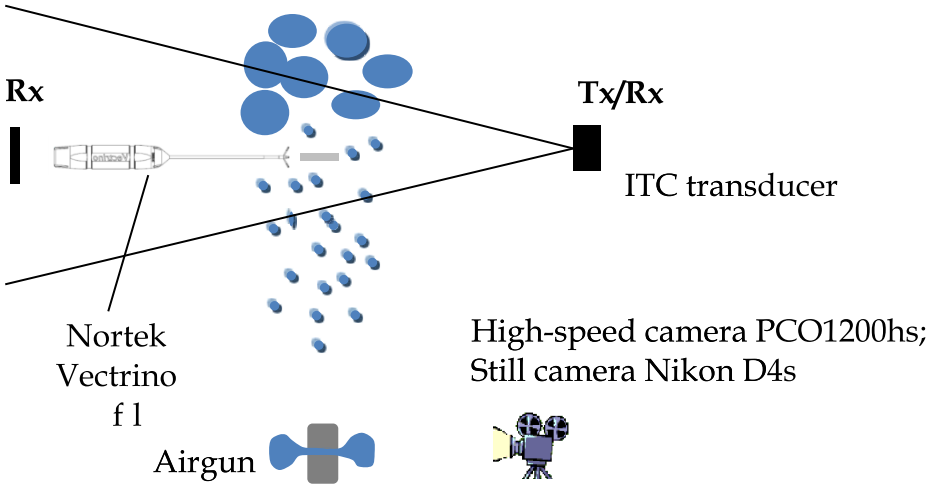

Figure 1. Illustration of the experiment set-up.

2.2 Airgun Description

The airgun used in the experiments was manufactured by Scientific Engineering Services (SES) of DST Group. The design was provided by Paul Brandner and Katrina de Graaf of the Australian Maritime College (AMC), who conducted research on the initial bubble

dynamics and pressure field generated by the airgun [3]. The design was slightly modified to fit the requirements of conducting experiments in the bigger tank of UASL.

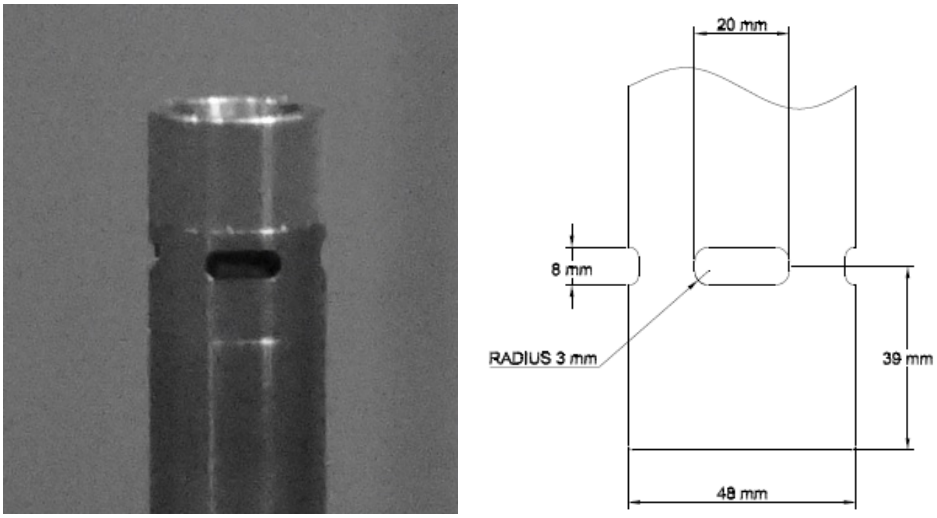

Figure 2. Airgun. Left: Image of the airgun; right: Major dimensions of the airgun.

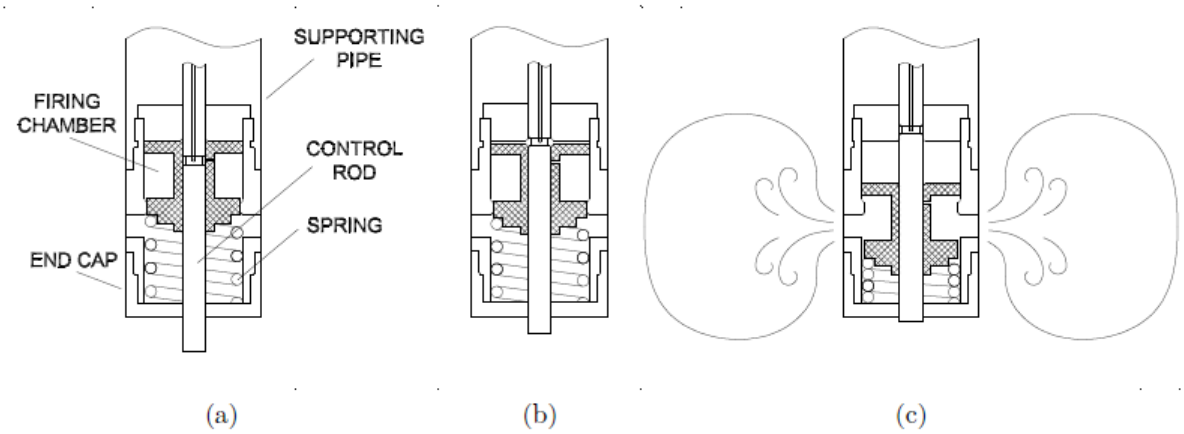

Figure 3. Illustration of airgun firing in three stages: (a) pressurised chamber under equilibrium; (b) equalisation of pressure across lower flange to fire shuttle and (c) release of air through ports to form bubble.

The underlying principle of an airgun relies on a firing chamber, filled with compressed gas, which is held shut via a pressure difference across the two ends of a shuttle. The lower flange of the shuttle in Figure 3 is larger than the upper flange. When the pressure difference across one end of the shuttle (in this case, the lower flange) is equalised (Figure 3), the shuttle can open and the compressed air in the firing chamber exhausts through several 'ports' in the body of the airgun, and forms the bubble.

2.3 Still Images

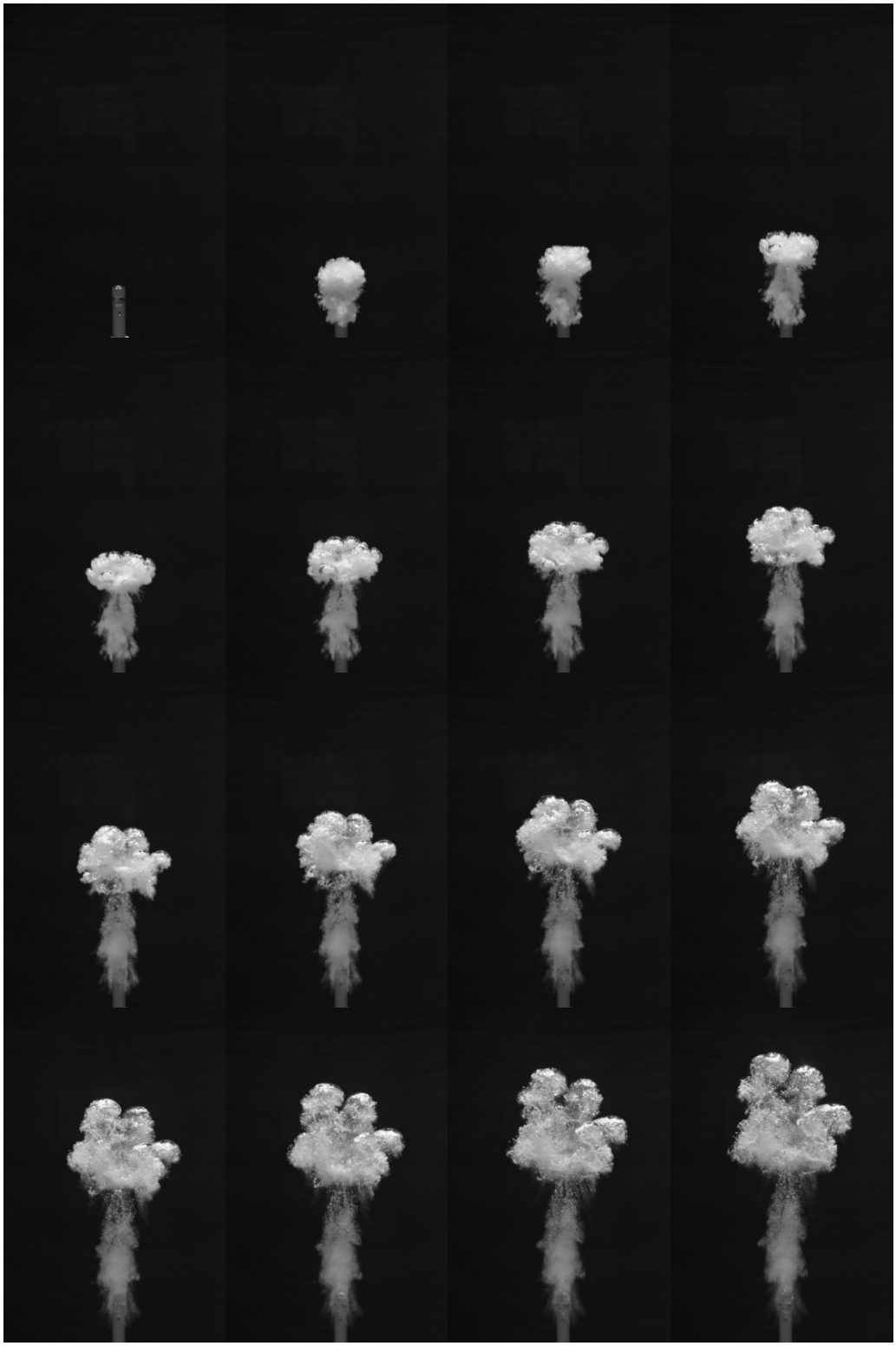

Figure 4. Sequence of still images of the rising bubble cloud. Time interval between images is 1/11 s. Initial pressure in the airgun is 6.89 MPa (1000 psi).

Still images of the rising bubble cloud, resulting from the airgun bubble break-up, have been obtained using a Nikon D4s digital SLR camera. An example of an image sequence is shown in Figure 4. The initial pressure in the airgun was 6.89 MPa (1000 psi). The frame rate was 11 frames per second. The exposure time is 1/8000 sec, the aperture is changed from f1.8 to f2.2 (shutter speed priority mode was used). A Zeiss prime lens Planar 1.4/85 ZF.2 with a focal length of 85 mm was used. The resolution of original images is 3280x4928 pixels.

The image sequence gives some insight into the development of the bubble cloud. The initial airgun bubble is not the same as an explosion bubble. The explosion bubble is an almost perfect sphere filled with gas [4], which then breaks into a cloud of small bubbles after three or four oscillations. The airgun bubble looks more like a foamy bubble. In other words, it is already a bubble cloud of very high volume fraction. Apparently, there is some distribution of bubbles in size, which is unfortunately impossible to measure at such a high volume fraction. One can see from the image sequence that there are very small bubbles that stay in the vicinity of the airgun while larger bubbles in the cloud rise quickly towards the water surface. It can also be noted that at the top of the bubble cloud the coalescence of bubbles takes place with very large bubbles formed.

Knowing the frame rate of the camera, we can extract the time history of the height of the top edge of the bubble cloud above the airgun. It is shown in Figure 5 along with its linear fit. One can see that the straight line fits the measurements very well, which means that the top edge of the bubble cloud is rising at practically constant velocity of 0.5 m/s. This rise velocity corresponds to the bubble diameter of 50 mm according to the most recent model of bubble terminal velocity [5]. Certainly we cannot conclude from this that the diameter of the bubble at the top of the bubble cloud is 50 mm. At such high volume fraction the model may not be accurate due to the interaction of bubbles in the cloud through water entrainment.

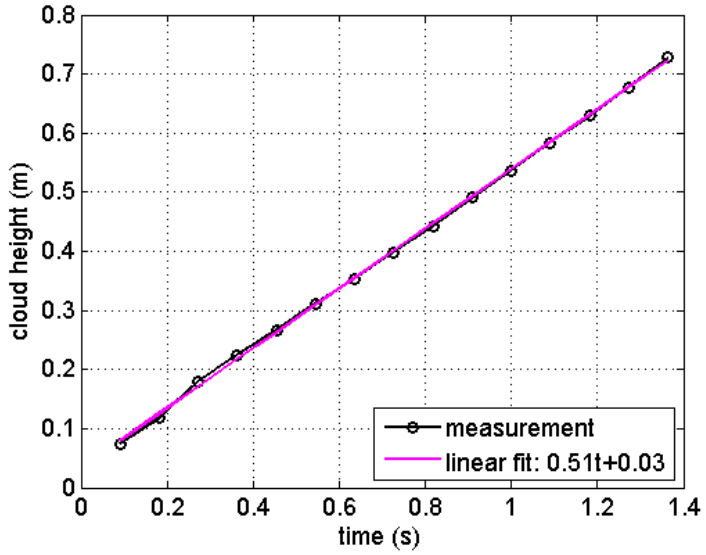

Figure 5. Time history of the top edge of the bubble cloud position above the airgun.

2.4 High-speed Videos

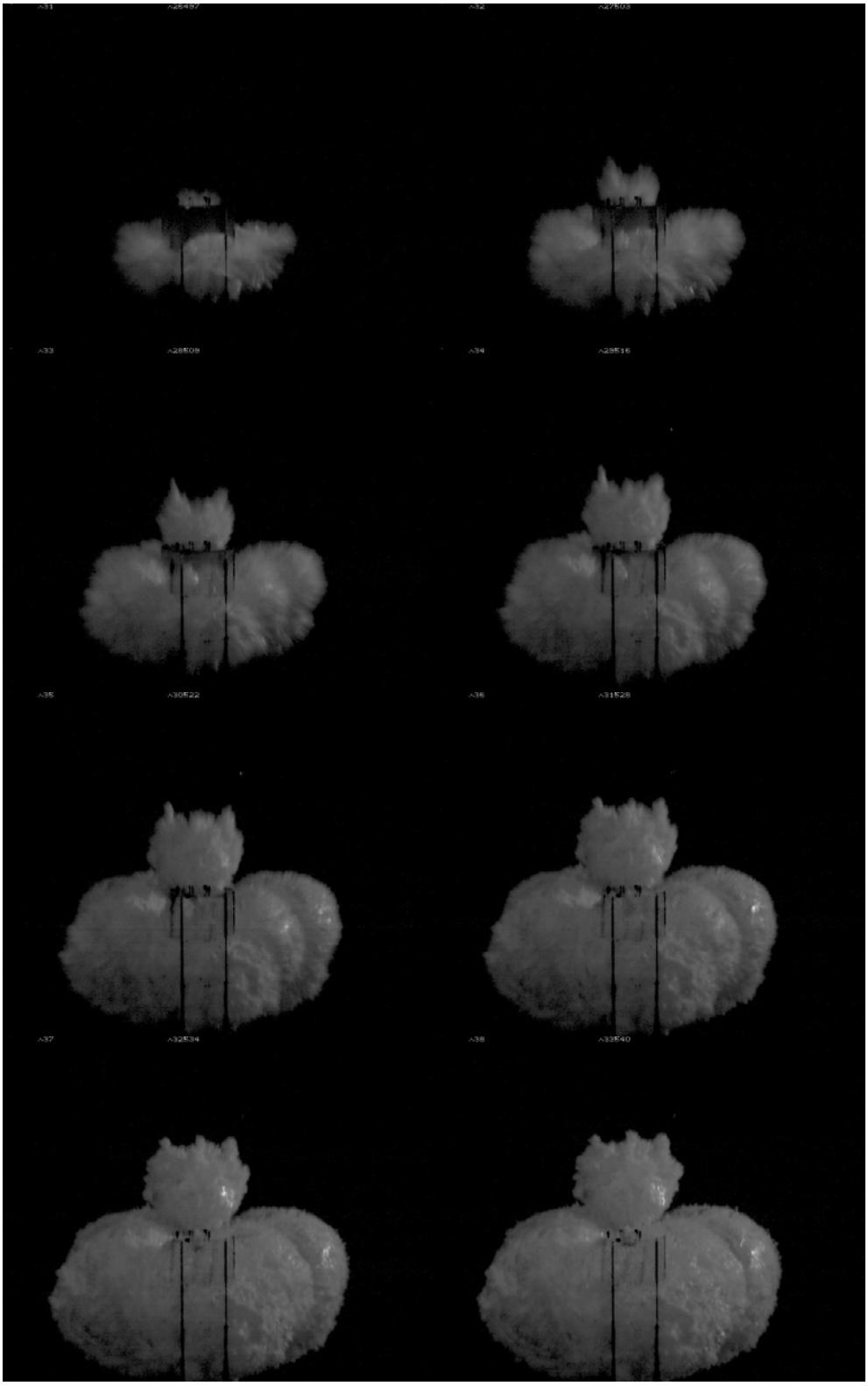

Figure 6. Sequential frames of high-speed video showing the initial bubble growth.

High-speed videos of the initial airgun bubble were obtained using a PCO1200hs camera. The full resolution of the camera is 1280 × 1024 pixels. The frame rate at full resolution is 500 fps. The frame rate can be increased by reducing the image resolution. In Figure 6, an example of a sequence of frames from a high-speed video of the initial bubble cloud is shown. The frame rate in this video was increased to 1000 fps by reducing the image resolution to 640 × 512 pixels. The initial pressure in the airgun was 6.89 MPa (1000 psi). The quality of images was improved by subtracting the background image, which was obtained by averaging several frames of the video before the air release. One can see from the images that the initial airgun bubble looks more like a bubble cloud of very high volume fraction, or like a foam bubble. It also has a four distinct lobes corresponding to four gas release ports in the airgun. This distinguishes the airgun bubble from the explosion bubble, which looks more like a perfect sphere for three or four oscillations before breaking up into a cloud of small bubbles [4].

Similar to the explosion bubble, the airgun bubble also undergoes several oscillations. By analysing video frame-by-frame in MATLAB® and making measurements of the bubble diameter, the time history of the bubble diameter were obtained for several runs. Since the airgun bubble is not a perfect sphere, we measured the diameter of the horizontal cross-section of the bubble. They are shown in Figure 7 for two different pressures of the airgun: 4.14 MPa (600 psi) and 6.89 MPa (1000 psi). Obviously the bubble at greater initial pressure grows to a larger size as can be seen from comparing the two plots. These results are compared with the model prediction later in the report.

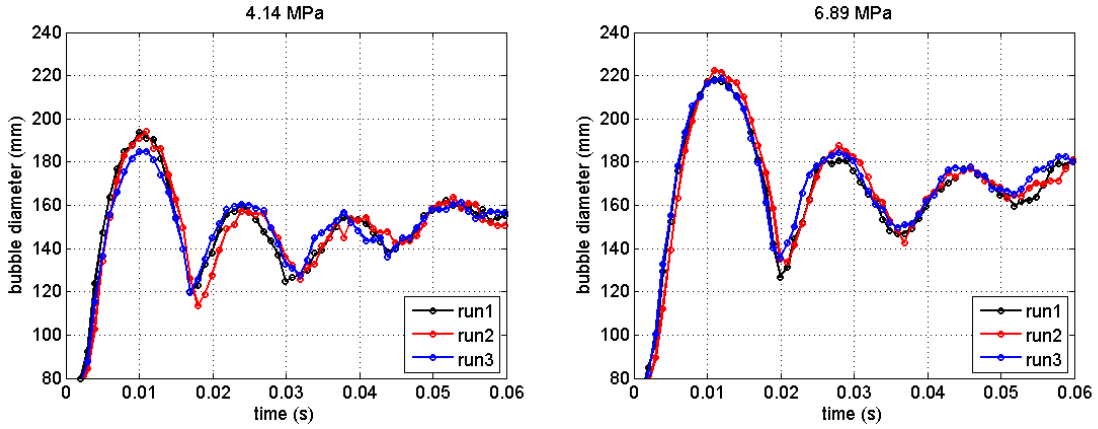

Figure 7. Time history of the airgun bubble diameter for different airgun pressure of 4.14 MPa (600 psi) (left plot) and 6.89 MPa (1000 psi) (right plot).

2.5 Velocimetry Data

In previously reported experiments with the compressed air canister [2] it was concluded that to explain the time history of the acoustic absorption in the bubble cloud one has to take into account the interaction between the bubbles of different size groups through entrained water. The bubbles of larger size rise faster than the small bubbles. Their rise entrains water which in turn drags smaller bubbles upward causing them to rise more quickly than in quiescent water. This results in a shorter dip in the time history of the acoustic transmission through the bubble cloud than predicted by the current UNDEX bubble cloud model, where it is assumed that bubbles of all sizes rise at their terminal velocity in still water [1]. It is not easy to calculate the velocity of the entrained water even in the case of a cloud of monodisperse bubbles [6]. In [6] the velocity of entrained water was modelled analytically as a step function and compared with the CFD simulations, which were obtained using a commercial CFD package ANSYS CFX. Further development of this approach may be required and will be considered in the modelling section of this report.

Given the complexity of the problem of the rise of the polydisperse high volume fraction bubble cloud, it is important for further model development to measure the velocity of the water entrained by the bubble cloud. It is, however, not straightforward to measure separately the velocity of entrained water and the velocity of the bubbles in the multiphase flows of high volume fraction. The use of Constant Temperature Anemometry (CTA) in such flows would be problematic. Contact of the CTA probe with bubbles would generate many non-physical spikes in the acquired signal, which presents a problem even in dilute gas-water flows [7]. The probe can be also damaged by frequent contact with bubbles and also by the shock wave generated by the airgun discharge.

In this experiment we used the Nortek Vectrino profiler, an acoustic Doppler velocimeter (Figure 8). It has a four-beam probe to measure three components of velocity over a range of 30 mm with the resolution of 1 mm (Figure 9) with an output rate of up to 100 Hz. The maximum value of measured velocity is 3 m/s. The measurement technique requires the presence of some particles in water to scatter sound back to the probe. Bubbles are good scatterers of sound, which makes an acoustic Doppler velocimeter a suitable instrument for measuring velocity in bubbly multiphase flows. This technique, however, measures velocity of the bubbles and not the velocity of entrained water. Only in the case of very small bubbles can we assume that the velocity of the bubbles coincides with the velocity of the water. Thus, in the plume type flow with which we deal in this experiment, the probe is first passed by the large bubbles. The velocity measured in the first moments of the passing plume is the velocity of large bubbles and not that of water entrained by them. The large bubbles rise to the surface very quickly and then small bubbles in the plume are dragged up by the water entrained by the larger bubbles. Thus, in the latter stages of the plume the measured velocity is that of entrained water.

Figure 8. Vectrino velocimeter (Nortek)

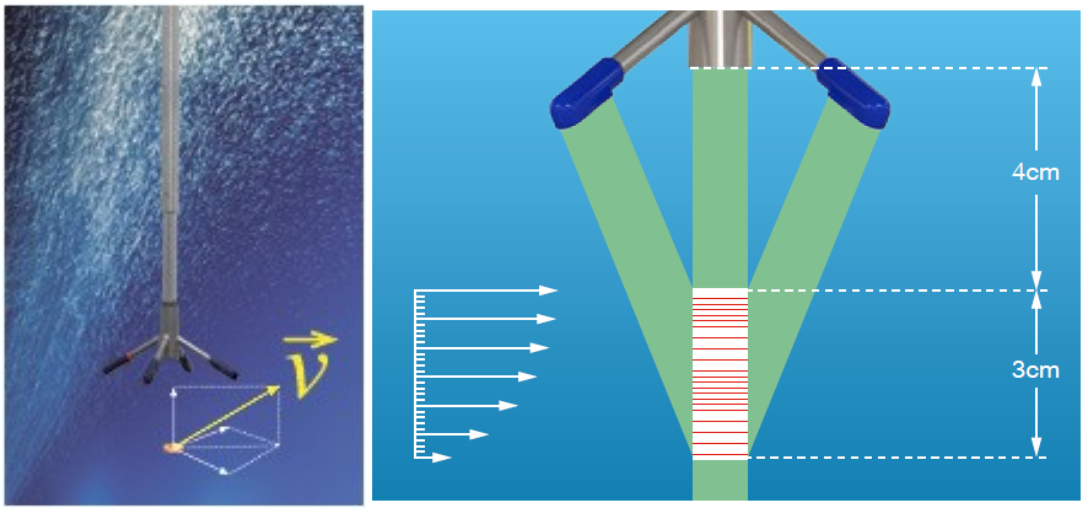

Figure 9. Nortek Vectrino velocimeter: principle of operation.

In this experiment the Vectrino profiler was placed horizontally with the sampling volume located approximately at the axis of the rising bubble cloud at the distance of 0.5 m above the airgun (Figure 1). The vertical component of the velocity is dominant in this flow. Its time history is shown for several runs in Figure 10 for initial pressure in the airgun of 4.14 MPa (600 psi) and in Figure 11 for the pressure of 6.89 MPa (1000 psi). In both figures the left plot shows data for individual runs, and the right plot displays the data averaged over those runs presented in the left plot.

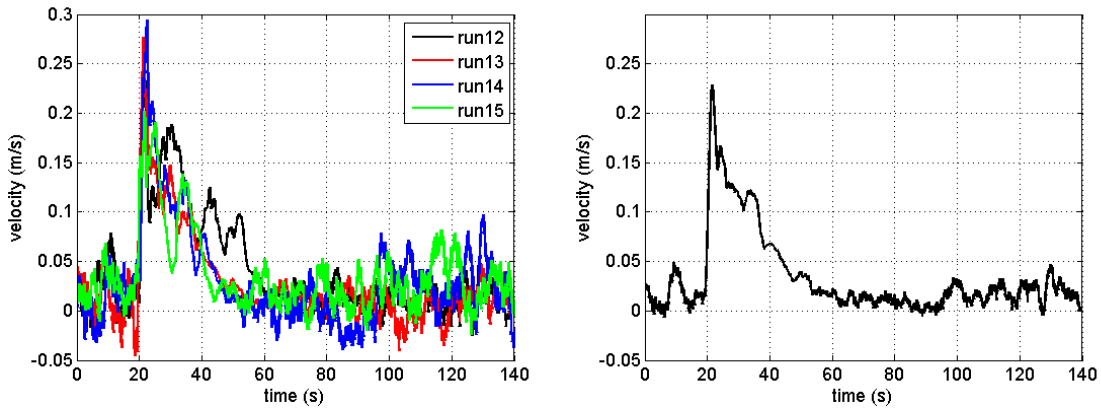

Figure 10. Vertical component of velocity in the bubble cloud 0.5 m above airgun. Left plot: velocity data for four different runs; right plot: velocity averaged over four runs. Initial pressure in the airgun is 4.14 MPa (600 psi).

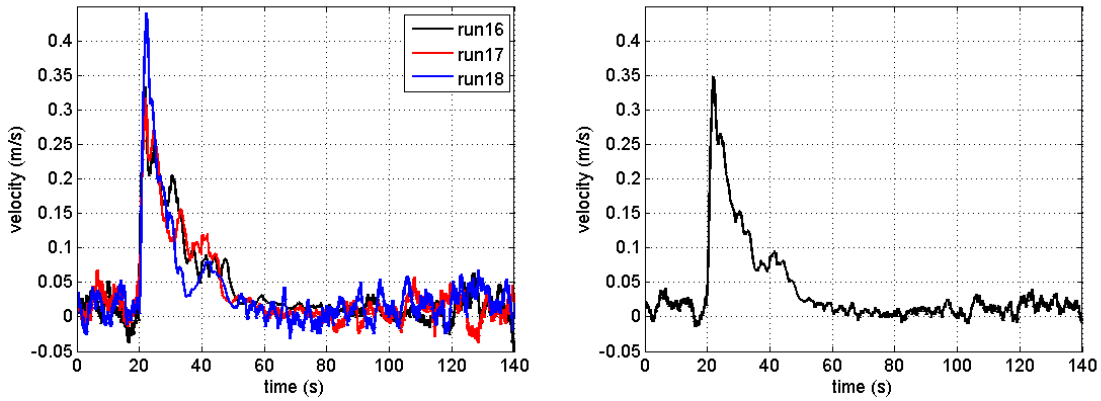

Figure 11. Vertical component of velocity in the bubble cloud 0.5 m above airgun. Left plot: velocity data for three different runs; right plot: velocity averaged over three runs. Initial pressure in the airgun is 6.89 MPa (1000 psi).

One can see from Figure 11 that the maximum velocity of the bubble front is about 0.45 m/s, which roughly corresponds to the value of 0.5 m/s inferred from the analysis of still images of the rising bubble cloud (Figure 4 and Figure 5).

2.6 Acoustic Transmission and Scattering

The measurements of acoustic properties of the bubble cloud are important from the point of view that they are related to the bubble size distribution in the cloud. One of the popular assumptions is that only those bubbles which are at resonance with the acoustic signal travelling through the bubble cloud contribute to its attenuation. In this approximation, also called the Resonant Bubble Approximation (RBA) [8], the bubble size distribution can be easily inferred from the measurement of the sound attenuation in an

appropriate range of acoustic frequency. There are also other more sophisticated methods of solving the inverse problem of determining the bubble size distribution from the measurements of acoustic attenuation [9], which attempt to take into account the contribution from the off-resonance bubbles. Such methods, however, are not always reliable. In this report we will use RBA to estimate the bubble size distribution from the acoustic data. For completeness we provide here a detailed description of this method.

First of all, we need to calculate the sound attenuation due to bubbles in the path between the transmitter and the receiver:

$$\alpha_{tot} = -20\log_{10}\left(\frac{A_{max}-A_{min}}{(A_{max}-A_{min})_{t=0}}\right), \tag{1}$$

where $A_{\min}, A_{\max}$ are the minimum and maximum values of the amplitude of the transmitted signal. This equation uses the fact that at $t = 0$ the bubbles have not yet reached the line between the transmitter and the receiver. As mentioned above, the main assumption of the RBA is that only those bubbles, which are at resonance with the insonifying field, contribute significantly to acoustic attenuation. In this case the bubble size distribution per unit volume can be expressed as [10]:

$$n(a_R) = \frac{\alpha_b \delta_R}{8.68\pi^2 a_R^3}, \tag{2}$$

where α_b is the attenuation due to bubbles expressed in dB/m, a_R is the resonant bubble radius at the insonifying frequency f, δ_R is the total damping constant at resonance,

$$\delta_{\mathrm{R}} = \delta_{\mathrm{Rr}} + \delta_{\mathrm{Rt}} + \delta_{\mathrm{Rv}}, \tag{3}$$

given by the sum of the reradiation term $\delta_{Rr} = ka_R$, the thermal damping term $\delta_{Rt} = d/b$, and the viscous damping term $\delta_{Rv} = 4\mu/(\rho_A \omega a_R^2)$. The resonant bubble radius at the given frequency f is calculated according to the following equation [10]:

$$a_R = \frac{1}{2\pi f}\sqrt{\frac{3\gamma b \beta P_A}{\rho_A}}, \tag{4}$$

where γ is the heat capacity ratio, P_A is the ambient pressure and ρ_A is the density of surrounding water. The parameters b and β are calculated from the following equations [10]:

$$\beta = 1 + \frac{2\sigma}{p_A a}\left(1 - \frac{1}{3\gamma b}\right), \tag{5}$$

$$b^{-1} = \left[1 + \left(\frac{d}{b}\right)^2\right]\left[1 + \left(\frac{3\gamma-3}{X}\right)\left(\frac{\sinh X - \sin X}{\cosh X - \cos X}\right)\right], \quad (6)$$

$$\frac{d}{b} = 3(\gamma - 1)\left[\frac{X(\sinh X + \sin X) - 2(\cosh X - \cos X)}{X^2(\cosh X - \cos X) + 3(\gamma - 1)X(\sinh X - \sin X)}\right], \quad (7)$$

$$X = a\left(\frac{2\omega\rho_g C_{pg}}{K_g}\right)^{1/2}. \quad (8)$$

In the above equations σ is the surface tension of the air-water interface, ρ_g is the bubble gas density, C_{pg} is the specific heat at constant pressure of bubble gas, and K_g is the thermal conductivity of bubble gas. Obviously, the parameters defined by the equations (5)-(8) themselves depend on the bubble radius. Therefore, equation (4) has to be solved numerically in conjunction with equations (5)-(8).

In this report we will also use the acoustic data for the validation of the model of the UNDEX bubble cloud. One of the outputs of this model is the bubble size distribution in the rising bubble cloud. This distribution is derived from the models of the initial bubble disintegration and subsequent bubble break-up by turbulence [1]. Knowing the bubble size distribution from the model we can solve the direct problem of calculating the attenuation of acoustic signal through the bubble cloud and compare it with the measurement.

The time history of acoustic transmission through the rising bubble cloud is shown in Figure 12 for the initial pressure in the airgun of 4.14 MPa (600 psi) and in Figure 14 for the initial pressure of 6.89 MPa (1000 psi). The line between the transmitter and the receiver passed through the axis of the bubble plume at 0.5 m above the airgun (Figure 1). The bubble cloud was insonified with short LFM pulses emitted from a high-frequency transducer. A custom built ITC transducer with centre frequency of 100 kHz was used in these experiments. The LFM pulse frequency range was from 20 to 240 kHz, with pulse duration of 770 μs. The sampling frequency was 5 MHz and the pulse repetition rate was 2.5 Hz. Both backscattered and transmitted signals through the bubble cloud were recorded. The results of this procedure are shown in Figure 13 for the case of an airgun pressure of 4.14 MPa (600 psi) and Figure 15 for airgun pressure of 6.89 MPa (1000 psi).

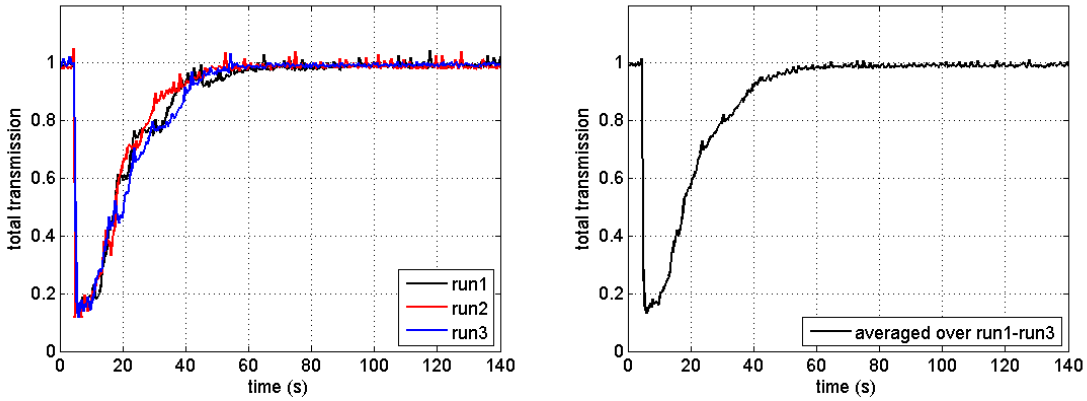

Figure 12. Time history of the total transmission through a rising bubble cloud. Left plot: three different runs; right plot: averaged over three runs. Initial pressure in the airgun is 4.14 MPa (600 psi).

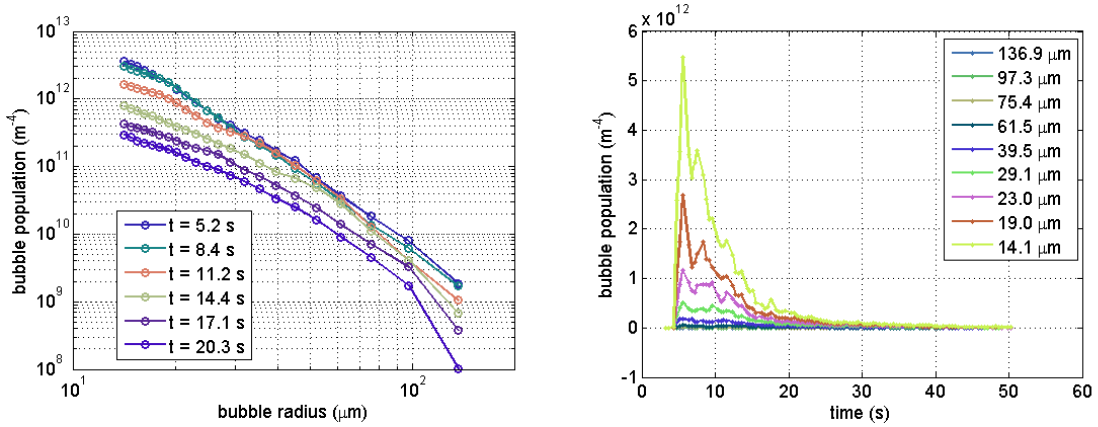

Figure 13. Inferred bubble size distribution for different time moments (left plot) and time history of bubble population for different bubble size groups (right plot). Initial pressure in the airgun is 4.14 MPa (600 psi).

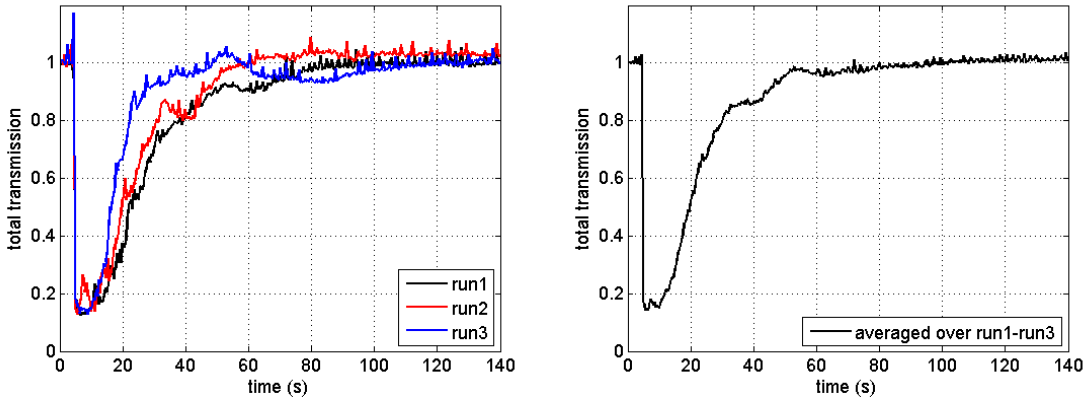

Figure 14. Time history of the total transmission through rising bubble cloud. Left plot: three different runs; right plot: averaged over three runs. Initial pressure in the airgun is 6.89 MPa (1000 psi).

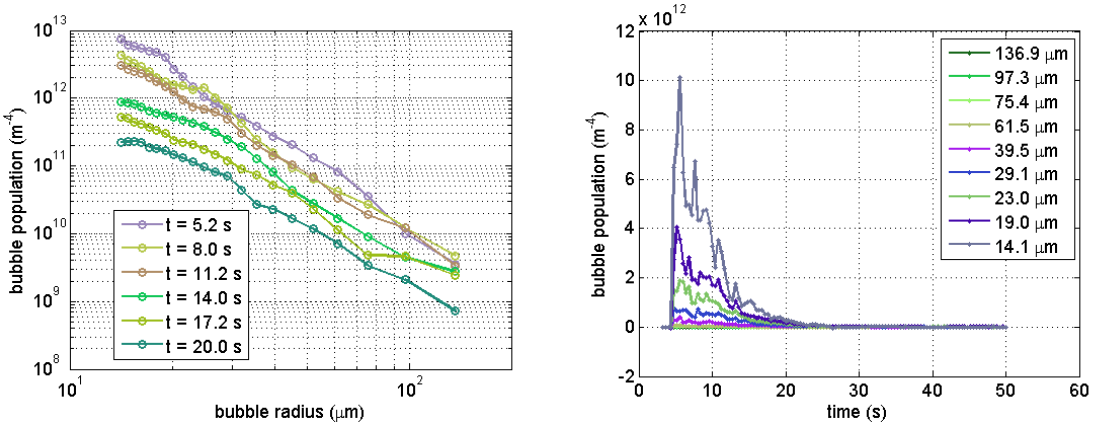

Figure 15. Inferred bubble size distribution for different time moments (left plot) and time history of bubble population for different bubble size groups (right plot). Initial pressure in the airgun is 6.89 MPa (1000 psi).

3. Modelling Aspects

3.1 Oscillation of Initial Bubble

In the previously developed model of the UNDEX remnant bubble cloud [1] the oscillation of the initial explosion bubble is based on the model described in [11]. The model is easily adapted to the airgun bubble. For completeness, we will present the main equations of the model here in detail.

The model is based on the doubly asymptotic approximation and combines relative simplicity based on the assumption of spherical shape of the explosion globe with the reasonable prediction of the globe oscillation damping. In our model of formation of the UNDEX remnant bubble cloud we employ the model of the explosion bubble oscillations from [11] with some modifications. Thus the radius of the spherical explosion globe, R , is described by the following equation:

$$R\ddot{R}f_1(\dot{R},\rho_l,\rho_g,c_l,c_g)+\frac{3}{2}\dot{R}^2f_2(\dot{R},\rho_l,\rho_g,c_l,c_g)+\dot{R}f_3(\dot{R},\rho_l,\rho_g,c_l,c_g)$$
$$=\frac{1}{\rho_l}f_4(p_\infty,p_{g0},R,\dot{R},\rho_l,\rho_g,c_l,c_g)+\frac{|\boldsymbol{u}-\boldsymbol{u}_b|^2}{4}, \tag{9}$$

where ρ_g, ρ_l is the density of gas inside the bubble and of the surrounding liquid, respectively, c_g, c_l is the speed of sound in gas and liquid, p_∞ is the ambient pressure of the surrounding fluid, and p_{g0} is the initial gas pressure inside the bubble. The functions in equation (9) are:

$$f_1=1+\zeta-\left(1-\frac{\rho_g}{\rho_l}\right)\frac{\dot{R}}{c_l}, \tag{10}$$

$$f_2=1+\frac{2}{3}\zeta-\frac{1}{3}\left(\frac{\dot{R}}{c_l}\right)+\frac{1}{3}\left(\frac{\rho_g}{\rho_l}\right)\left(1+\frac{\dot{R}}{c_l}+\frac{R\dot{p}_g}{c_l\rho_g}\right), \tag{11}$$

$$f_3=\zeta c_l+\zeta\dot{R}, \tag{12}$$

$$f_4=\left(P_g-p_\infty\right)\left(1+\frac{\dot{R}}{c_l}\right)+\frac{R}{c_l}\dot{P}_g. \tag{13}$$

In the above equations $\zeta=\rho_g c_g/\rho_l c_l$ is the specific acoustic impedance ratio. The gas pressure inside the bubble, $P_g=p_{g0}(V_0/V)^\gamma$, where V_0 is the volume of the airgun chamber, $V=(4\pi/3)R^3$ is the volume of the bubble, γ is the polytropic index of the bubble gas, which varies between 1 (isothermal) and 1.4 (adiabatic). We assume the value of 1 in

this work. The ambient pressure of the surrounding fluid is calculated at the depth of the bubble centre, d_{bc}, as $p_\infty = p_{atm} + \rho_l g d_{bc}$.

The second term on the right-hand side of the equation (9) is due to the added pressure on the bubble surface resulting from the bubble motion [12]. We include this term in addition to the model provided in [11]. The initial conditions for the equation (9) are:

$$R(0) = (3V_0/4\pi)^{1/3}, \dot{R}(0) = 0. \tag{14}$$

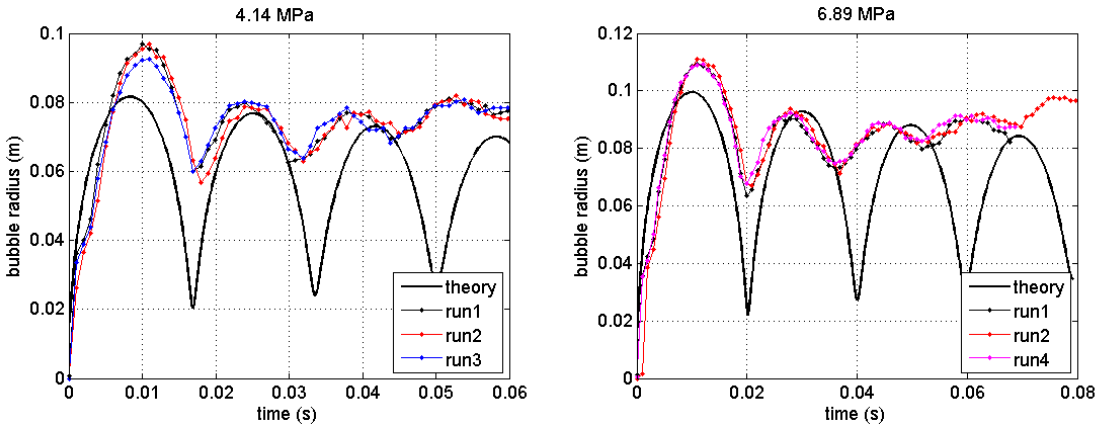

Figure 16. Comparison of theory with experiment for oscillations of the initial bubble. Left plot: initial pressure in the airgun is 4.14 MPa (600 psi), Right plot: initial pressure is 6.89 MPa (1000 psi).

3.2 Initial Bubble Break-up into Bubble Cloud

The initial bubble break-up into the cloud of smaller bubbles is modelled here as in the previously developed model [1]. Again, for completeness, we reproduce the model of initial bubble fragmentation here in detail.

We assume that the explosion globe break-up occurs at the third minimum as a result of instability of the bubble spherical shape. It is a simplification, because in reality the fragmentation of the explosion globe occurs in steps at the second, third, and even fourth minimum of the breathing modes, which could be seen from the video sequence [4]. However, we believe that compressing this process into one single act of fragmentation is a reasonable assumption which significantly simplifies the model. The model improvement in this respect may be addressed in future work.

Just before the explosion globe break-up its radius is R_0^* and the gas pressure inside the bubble p_{g0}^*. In the current model we obtain these values from the solution of equations in the previous section. Alternatively, they can be obtained from a more accurate numerical model of an underwater explosion.

We estimate initial bubble size distribution from the modes of the Rayleigh-Taylor instability for the spherical bubble. The growth rate of the non-spherical distortions on the bubble surface is proportional to the following value [13]:

$$f(m) = (m-1)[\Gamma - (m+1)(m+2)], \tag{15}$$

where $\Gamma = \rho R^2 \ddot{R}/\sigma$ and m is the order of a spherical harmonic distortion. We postulate that each mode m leads to bubbles of size $r_m = R_0^*/m$ in the daughter bubble cloud and that the number of bubbles of this size is proportional to the function $f(m)$:

$$n_m = A(m-1)[\Gamma_0^* - (m+1)(m+2)] = A\left(\frac{R_0^*}{r_m} - 1\right)\left[\Gamma_0^* - \left(\frac{R_0^*}{r_m} + 1\right)\left(\frac{R_0^*}{r_m} + 2\right)\right], \tag{16}$$

where Γ_0^* is the value of Γ at $R = R_0^*$. The normalisation coefficient A is determined from the balance of the gas volume:

$$\sum_m n_m \Delta r_m r_m^3 = (R_0^*)^3. \tag{17}$$

We assume that straight after the break-up the gas in the daughter bubbles has the same pressure, p_{g0}^*, as the explosion bubble just before break-up. The bubbles then expand to reach the balance with the pressure in the surrounding fluid. The new bubble size can be obtained from the following equation:

$$p_1 V_1 = p_2 V_2, \tag{18}$$

where $p_1 = p_{g0}^*$ and $p_2 = p_a + \rho g h_b + 2\sigma/\tilde{r}_m$, h_b being the depth of the bubble, and p_a the atmospheric pressure. This results in the following cubic equation for the new bubble radius, $\tilde{r}_m$:

$$\tilde{r}_m^3 + \frac{2\sigma}{p_a + \rho g h_b}\tilde{r}_m^2 - \frac{p_{g0}^*}{p_a + \rho g h_b} r_m^3 = 0. \tag{19}$$

If the surface tension can be neglected, this equation simplifies significantly:

$$\tilde{r}_m = r_m \left(\frac{p_{g0}^*}{p_a + \rho g h_b}\right)^{1/3}. \tag{20}$$

However, with modern computers solving the cubic equation does not affect the overall computation time noticeably. The new bubble size distribution is calculated as:

$$\tilde{n}_m = n_m \frac{\Delta r_m}{\Delta \tilde{r}_m}, \tag{21}$$

and the new total volume of the bubbles in the cloud is:

$$\tilde{V} = \left(\frac{4\pi}{3}\right) \sum_m \tilde{n}_m \Delta \tilde{r}_m \tilde{r}_m^3. \tag{22}$$

The radius of the bubble cloud can be estimated as follows:

$$\tilde{R} = \alpha_C \left(\frac{3\tilde{V}}{4\pi}\right)^{1/3}. \tag{23}$$

Currently we consider α_C as an empirical parameter, where $\alpha_C > 1$.

Continuing with the example from the previous section and assuming $\alpha_C = 1.5$, we obtain the bubble size distribution shown in Figure 17.

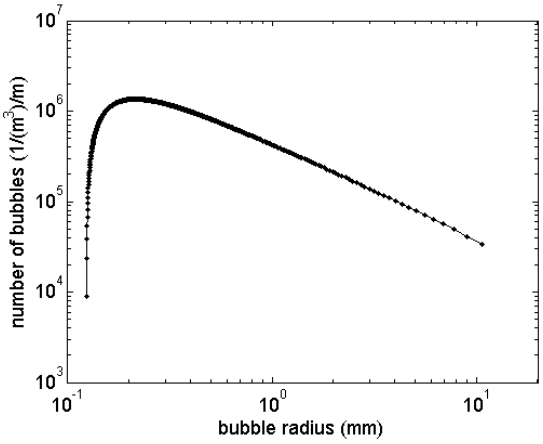

Figure 17. Estimated bubble size distribution after the initial break-up of the explosion bubble. Initial pressure 6.89 MPa (1000 psi).

3.3 Turbulence Resulting from Explosion Bubble Break-up

We assume that almost all potential energy of the explosion bubble before break-up transfers into the turbulent kinetic energy, which then gradually decays due to dissipation, further breaking the bubbles in the remnant bubble cloud. The potential energy of the compressed explosion globe is computed as work performed against external pressure during globe adiabatic expansion from the compressed state to the state of equilibrium with the external pressure [14]:

$$\Pi = 4\pi \int_{R_0}^{R_1} [p(r) - P_\infty] r^2 dr. \tag{24}$$

Here $P_\infty = p_a + \rho g h_b$ is the ambient pressure at the bubble depth h_b. During adiabatic expansion the pressure inside the bubble is changing according to the following equation:

$$p(r) = P_0 \left(\frac{R_0}{r}\right)^{3\gamma}. \tag{25}$$

Obviously, R_1 is obtained from equation (25) when $p(R_1) = P_\infty$. Integration of (24) will give the following equation for the bubble potential energy:

$$\Pi = \frac{4\pi}{3} R_0^3 \left\{ \frac{P_0}{1-\gamma} \left[\left(\frac{P_0}{P_\infty}\right)^{\frac{1-\gamma}{\gamma}} - 1 \right] - P_\infty \left[\left(\frac{P_0}{P_\infty}\right)^{\frac{1}{\gamma}} - 1 \right] \right\}. \tag{26}$$

When a bubble breaks its potential energy mainly goes into the kinetic energy of the fluid creating a turbulent spot with total kinetic energy of

$$K_0 = \beta_K \Pi, \tag{27}$$

where $\beta_K < 1$ accounts for energy loss due to change in surface energy and acoustic radiation. In the current research we neglect these losses and assume $\beta_K \approx 1$. We assume also that the initial radius of the turbulent spot coincides with the radius of the bubble cloud, $\tilde{R}$. Thus the initial condition for the turbulent kinetic energy per unit mass is:

$$k = \begin{cases} k_0, & r \le \tilde{R} \\ 0, & r > \tilde{R} \end{cases}, \tag{28}$$

where

$$k_0 = \frac{3K_0}{4\pi\rho(1-\alpha_C^{-3})\tilde{R}^3}.$$

The decay of the turbulent kinetic energy is described by the following equation [15]:

$$\frac{\partial k}{\partial t} = -C_\mu \frac{k^{3/2}}{l} + \frac{1}{r^2}\frac{\partial}{\partial r}\left[\frac{\sqrt{k}l}{\sigma_k} r^2 \frac{\partial k}{\partial r}\right]. \tag{29}$$

For the turbulent parameters in this equation we use the following standard values: $C_\mu = 0.09, \sigma_k = 1, l = 2\tilde{R}$. Equation (29) is solved numerically using the Crank-Nicolson finite difference method. The dissipation rate of the turbulent kinetic energy, which is used further in the model of the bubble break-up, is calculated according to the following equation:

$$\varepsilon = C_\mu \frac{k^{3/2}}{l}. \tag{30}$$

Continuing with the example, Figure 18 shows the decay of the turbulent kinetic energy at the centre of the turbulent spot obtained from the numerical solution of equation (29).

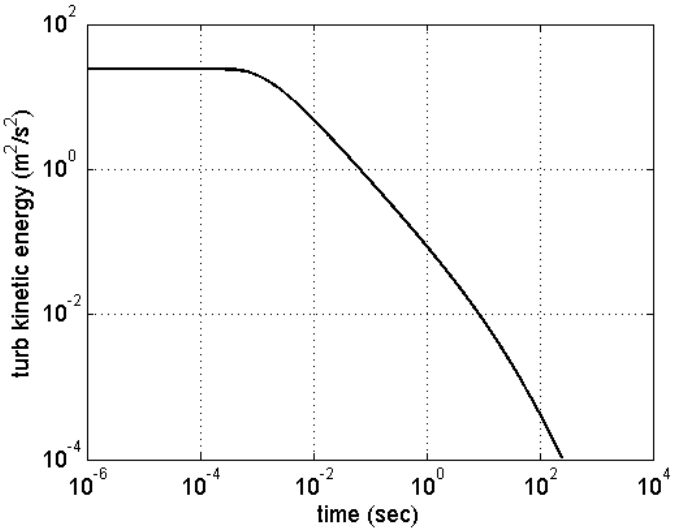

Figure 18. Decay of the turbulent kinetic energy at the centre of the turbulent spot. Initial pressure 6.89 MPa (1000 psi).

3.4 Further Bubble Break-up by Turbulence

The change of the bubble size distribution, n, due to bubble break-up by turbulence is described by the following equation [16]:

$$\frac{\partial n}{\partial t} = \int_D^\infty m(D_0) f(D, D_0) g(D_0) n(D_0)\, dD_0 - g(D) n. \tag{31}$$

The first term on the right-hand side of this equation describes the birth rate of bubbles of diameter D; the second term is the death rate of bubbles of this size. In this equation, $g(D)$ is the break-up frequency, $f(D, D_0)$ is the probability density function of the daughter bubbles resulting from the break-up of the mother bubble of size D_0, $m(D_0)$ is the average number of daughter bubbles per one break-up event. Here we use the break-up frequency and daughter bubbles probability density function from [17, 18]:

$$g(\varepsilon, D_0) = K_g D_0^{-1} \sqrt{\beta(\varepsilon D_0)^{2/3} - 12\frac{\sigma}{\rho D_0}}, \tag{32}$$

$$f(D, D_0) = B\left[\frac{1}{2}\rho\beta(\varepsilon D)^{2/3} - \frac{6\sigma}{D_0}\right]\left[\frac{1}{2}\rho\beta(\varepsilon D_2)^{2/3} - \frac{6\sigma}{D_0}\right]. \tag{33}$$

In the above equations ε is the dissipation rate of the turbulent kinetic energy, K_g and β are empirical constants, $D_2 = (1 - D^3)^{1/3}$ is the size of the second daughter bubble, and B is the normalisation factor. The values for the empirical constants, $K_g \approx 0.25$ and $\beta = 8.2$, are suggested in [17, 18].

Applying the turbulent kinetic energy obtained in the previous section to the bubble cloud with the initial bubble size distribution from Figure 17 we obtain the final bubble size distribution in the bubble cloud shown in Figure 19.

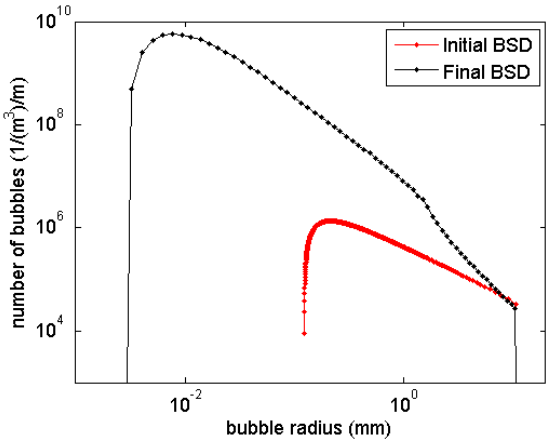

Figure 19. Final bubble size distribution after break-up by turbulence. Initial pressure 6.89 MPa (1000 psi).

3.5 Bubble Cloud Rise

Previously [1] we modelled the rise of bubble cloud assuming one-way coupling, i.e. that the bubbles do not affect the ambient fluid. In other words the bubble cloud was modelled as an assembly of non-interacting individual bubbles rising in quiescent water with their respective terminal velocities. This approximation is justified at relatively low volume fraction of bubbles. At higher values of the gas volume fraction the momentum transfer from the disperse bubble phase to the ambient water may be significant, which will induce the motion of the water and this will in turn affect the rise velocity of the bubbles. Thus the cloud of bubbles will rise at a faster speed than the terminal speed of a single bubble. Therefore, at higher values of the gas volume fraction the model of bubble cloud rise should take into account the two-way coupling between disperse and continuous phases. The two-way coupling is difficult to implement in the Lagrangian formalism, which is better suited for the one-way coupling approximation. Therefore, in this research we employ the Eulerian-Eulerian approach.

3.5.1 Governing equations

In the Eulerian-Eulerian formalism each phase is treated as a continuum, for which the continuity and momentum equations are [19]:

$$\frac{\partial}{\partial t}(\varphi_\alpha \rho_\alpha) + \nabla \cdot (\varphi_\alpha \rho_\alpha \boldsymbol{U_\alpha}) = S_\alpha + \Gamma_\alpha \tag{34}$$

$$\frac{\partial}{\partial t}(\varphi_\alpha \rho_\alpha \boldsymbol{U_\alpha}) + \nabla \cdot \left(\varphi_\alpha (\rho_\alpha \boldsymbol{U_\alpha} \otimes \boldsymbol{U_\alpha})\right) = -\varphi_\alpha \nabla p_\alpha + \nabla \cdot \left(\varphi_\alpha \mu_\alpha (\nabla \boldsymbol{U_\alpha} + (\nabla \boldsymbol{U_\alpha})^T)\right) + \sum_{\beta=1}^{N_p} \left(\Gamma^+_{\alpha\beta} \boldsymbol{U}_\beta - \Gamma^+_{\beta\alpha} \boldsymbol{U}_\alpha\right) + \boldsymbol{S}_{M\alpha} + \boldsymbol{M}_\alpha \tag{35}$$

In the above equations α is the phase index, $1 \le \alpha \le N_p$, N_p is the total number of phases, φ_α is the volume fraction of the phase α, S_α is an external mass source of the phase α, Γ_α is the mass source of phase α due to interphase mass transfer. The source term $\boldsymbol{M}_\alpha$ describes the momentum exchange due to interfacial forces acting on phase α from all other phases. The source term $\boldsymbol{S}_{M\alpha}$ refers to external body forces. The term $\sum_{\beta=1}^{N_p}\left(\Gamma^+_{\alpha\beta}\boldsymbol{U}_\beta - \Gamma^+_{\beta\alpha}\boldsymbol{U}_\alpha\right)$ describes momentum transfer caused by interphase mass transfer. In the current research, however, we do not consider the interphase mass transfer and neglect the latter term and the term Γ_α in the continuity equation. There are also no external sources of mass, i.e. $S_\alpha = 0$.

In the case of the cloud of monodisperse bubbles we have only two phases: water and gas bubbles of uniform size, d_p. Let us denote the volume fraction of gaseous phase as φ. Then the volume fraction of water is $1 - \varphi$. We also use subscript w to denote parameters relevant to water, and subscript g for the bubbly phase parameters. With this, the

momentum equation for the bubble phase is

$$\begin{gathered}\frac{\partial}{\partial t}\left(\varphi\rho_g \boldsymbol{U}_g\right)+\nabla\cdot\left(\varphi\left(\rho_g \boldsymbol{U}_g\otimes\boldsymbol{U}_g\right)\right)= \\ -\varphi\nabla p+\nabla\cdot\left(\varphi\mu_g\left(\nabla\boldsymbol{U}_g+\left(\nabla\boldsymbol{U}_g\right)^T\right)\right)+\varphi\rho_g\boldsymbol{g}-\boldsymbol{M}_D\end{gathered} \tag{36}$$

and water

$$\begin{gathered}\frac{\partial}{\partial t}\left((1-\varphi)\rho_w\boldsymbol{U}_w\right)+\nabla\cdot\left((1-\varphi)(\rho_w\boldsymbol{U}_w\otimes\boldsymbol{U}_w)\right)= \\ -(1-\varphi)\nabla p+\nabla\cdot\left((1-\varphi)\mu_w(\nabla\boldsymbol{U}_w+(\nabla\boldsymbol{U}_w)^T)\right)+(1-\varphi)\rho_w\boldsymbol{g}-\boldsymbol{M}_D\end{gathered} \tag{37}$$

Here the source term $\boldsymbol{M}_D$ describes the interfacial momentum transfer due to drag force.

Even in a relatively simple case of the cloud of monodisperse bubbles it is not possible to find an exact analytical solution of equations (36) and (37). We will analyse this problem numerically using the commercial CFD package ANSYS CFX and will also develop a simplified numerical model.

3.5.2 Simplified model of water entrainment

In the simplified model we assume that the flow is axisymmetric, the bubble cloud consists of monodisperse bubbles, the bubbles in the cloud are rising at constant slip velocity defined by their size and assumed drag model. The influence of entrained water on the shape of the bubble cloud is described by a simple model. The equation (37) of water velocity components in cylindrical coordinates are

$$\begin{gathered}\frac{\partial u}{\partial z}+\frac{1}{r}\frac{\partial}{\partial r}(rv)=0, \\ \frac{\partial u}{\partial t}+u\frac{\partial u}{\partial z}+v\frac{\partial u}{\partial r}=\nu_w\left[\frac{\partial^2 u}{\partial z^2}+\frac{1}{r}\frac{\partial}{\partial r}\left(r\frac{\partial u}{\partial r}\right)\right]+\frac{M_D^{(z)}}{(1-\varphi)\rho_w}, \\ \frac{\partial v}{\partial t}+u\frac{\partial v}{\partial z}+v\frac{\partial v}{\partial r}=\nu_w\left[\frac{\partial^2 v}{\partial z^2}+\frac{1}{r}\frac{\partial}{\partial r}\left(r\frac{\partial v}{\partial r}\right)-\frac{v}{r^2}\right]+\frac{M_D^{(r)}}{(1-\varphi)\rho_w}.\end{gathered} \tag{38}$$

In the above equations the interfacial momentum transfer due to drag force has the form:

$$M_D^{(z)}=\frac{3}{4}\frac{C_D}{d_b}\varphi_g\rho_w U_s^2,\quad M_D^{(r)}=0, \tag{39}$$

where C_D and U_s are the drag coefficient and the slip velocity of the bubble of diameter d_b, respectively.

The gas volume fraction, φ_g, is assumed to remain constant inside the bubble cloud and zero outside it:

$$\varphi_g = \begin{cases} \varphi_0, & if \ \ (r/r_c)^2 + (z/z_c)^2 \le 1 \\ 0, & otherwise \end{cases} \tag{40}$$

In the simplified model, the bubble cloud shape is approximated by an oblate spheroid (Figure 20). We assume that the initial shape of the bubble cloud is spherical, $r_c = z_c = r_{c0}$, which is estimated from equation (23) above.

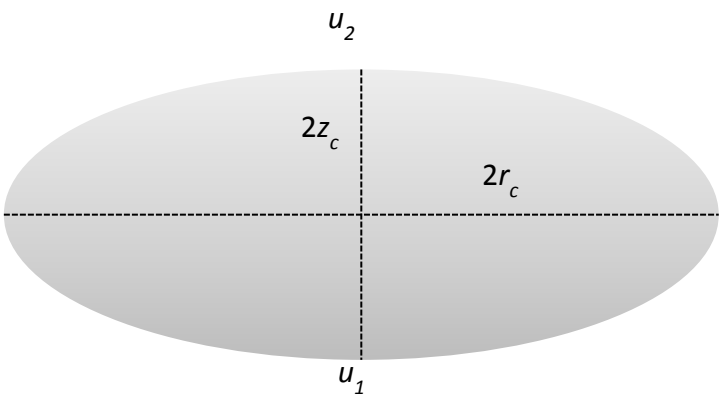

Figure 20. Simple model of bubble cloud shape.

During the rise of the bubble cloud, the water velocity at the bottom of the cloud, u_1, is higher than that at the top, u_2. This will lead to the gradual flattening of the spheroid. The vertical axis of the oblate spheroid can be estimated from the following equation:

$$z_c(t + \Delta t) = z_c(t) + \alpha(u_2 - u_1)\Delta t, \tag{41}$$

where $\alpha \le 0.5$. We also assume that the total volume of the bubble cloud remains constant:

$$V_c = \frac{4}{3}\pi r_c^2 z_c = const, \tag{42}$$

from which we find the horizontal semi-axis of the spheroid, r_c. Such an estimation of the shape of the bubble cloud can lead to excessive non-physical flattening, especially at high

volume fractions. To overcome this without complicating the model, we set a minimum for the spheroid aspect ratio, $\varepsilon_c = z_c/r_c$. In our simulations we usually assumed $\varepsilon_{cmin} = 1/8$.

The speed of the bubble cloud rise is calculated as the sum of the bubble slip velocity, U_s, and the water velocity averaged over the vertical axis of the spheroid. To account for non-uniformity of the water velocity over the whole volume of the bubble cloud, we introduce some scaling factor $\beta \leq 1$:

$$U_c = U_s + \beta u_{cm}, \tag{43}$$

where

$$u_{cm} = \frac{1}{2z_c}\int_{z_{ct}-z_c}^{z_{ct}+z_c} u(z, r = 0)dz. \tag{44}$$

Here z_{ct} is the position of the centre of the spheroid calculated at each time step as

$$z_{ct}(t + \Delta t) = z_{ct}(t) + u_{cm}\Delta t, \tag{45}$$

Figure 21 and Figure 22 compare the simplified model of water entrainment by a rising cloud of monodisperse bubbles with corresponding numerical simulations using the ANSYS CFX package.

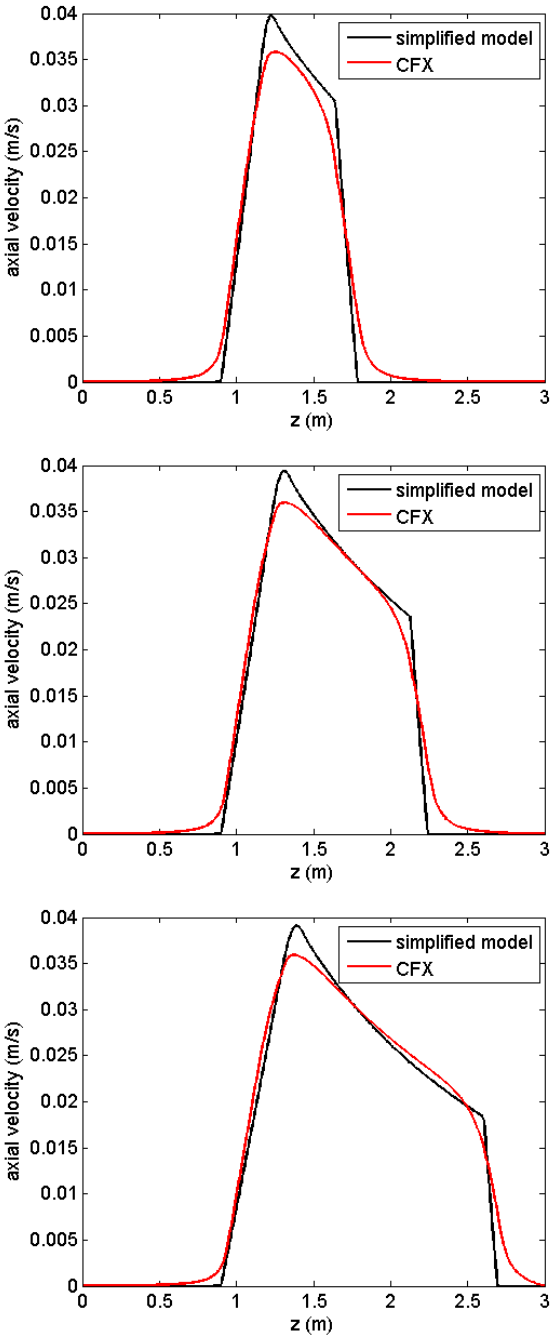

Figure 21. Axial velocity of water entrained by rising bubble cloud at different time moments, from top down: 3 s, 5 s, 7 s.
Bubble diameter is 9.68 mm, gas volume fraction is 0.00458.

The plots show the velocity of entrained water at the vertical axis of the rising bubble cloud at different moments of time from the start of the cloud rise. The results shown in Figure 21 correspond to the case of low gas volume fraction of $4.58 \cdot 10^{-3}$ and relatively

small bubble diameter of 9.68 mm. One can see a good agreement between the simplified model and high fidelity CFD simulations.

The agreement is not that good in the case of high gas volume fraction of 0.29 and large bubble diameter of 62.5 mm, results for which are shown in Figure 22.

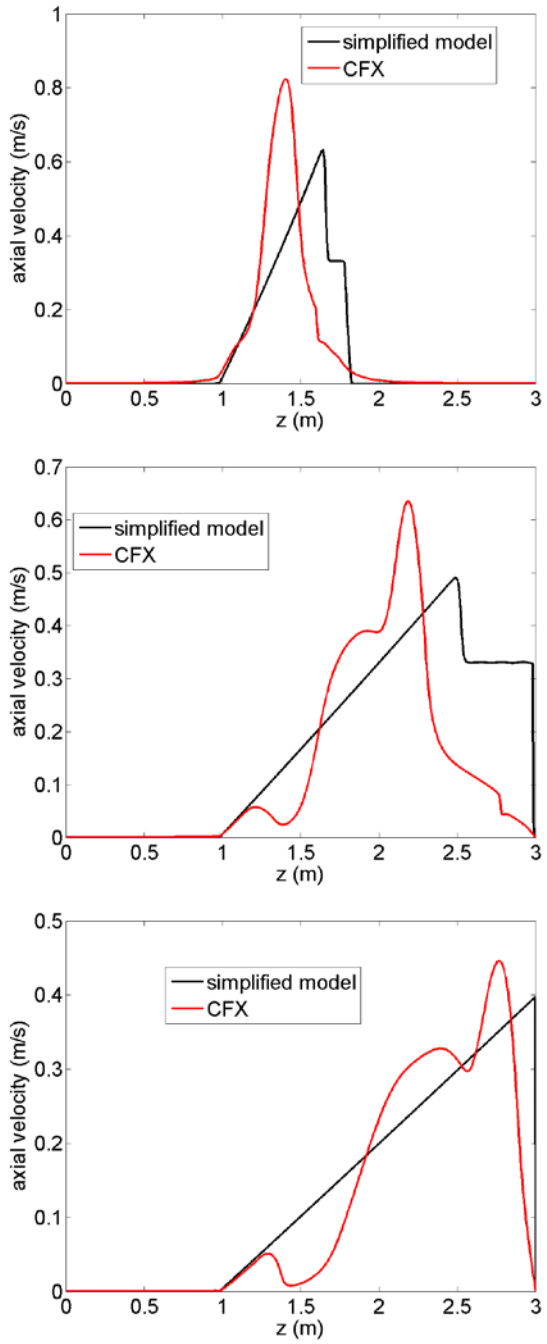

Figure 22. Axial velocity of water entrained by rising bubble cloud at different time moments, from top down: 1 s, 3 s, 5 s.
Bubble diameter is 62.5 mm, gas volume fraction is 0.29.

4. Application of the Simplified Model to the Airgun Bubble Cloud

In the above simplified model of water entrainment by a bubble cloud we assume that the bubble cloud consists of monodisperse bubbles. To apply this model to the rise of an airgun bubble cloud, where bubbles are distributed in quite a wide range of sizes (Figure 19), we make the following assumptions. We assume that all bubbles in the cloud are divided into 'large' and 'small' bubbles. 'Large' bubbles entrain water, and 'small' bubbles are entrained by water. To select the bubble size which divides the bubbles into 'large' and 'small' fraction, let us consider the bubble terminal velocity as a function of the bubble diameter (Figure 23). In this plot the terminal velocity is obtained from the balance of buoyancy and drag forces, in which the Grace Drag model is used. From this plot we can see that below a certain bubble diameter of about 2.7 mm the bubble velocity is decreasing sharply. We select this bubble size as the division between the 'large' and 'small' fractions.

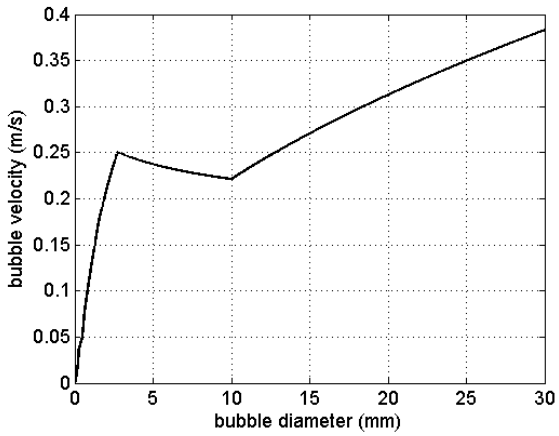

Figure 23. Bubble terminal velocity obtained from the Grace Drag model.

Because the simplified model of water entrainment assumes the monodisperse bubbles, we model the whole fraction of 'large' bubbles as a monodisperse fraction with an effective bubble size, for which we select the mean bubble diameter in the 'large' bubble fraction.

In this section we will consider the case of the airgun with the initial air pressure of 1000 psi. The bubble size distribution in the cloud after break-up of the initial airgun bubble is obtained from the models described above and presented in Figure 19. In this case the effective bubble size of 'large' bubbles in a representative monodisperse fraction is 10.6 mm and its volume fraction is 0.287. Using these parameters in the simplified model of water entrainment by the bubble cloud, we obtain the velocity field in the water column as a function of time and spatial coordinates. Comparison of the water velocity at the axis of the bubble cloud with the measurements is presented in Figure 24.

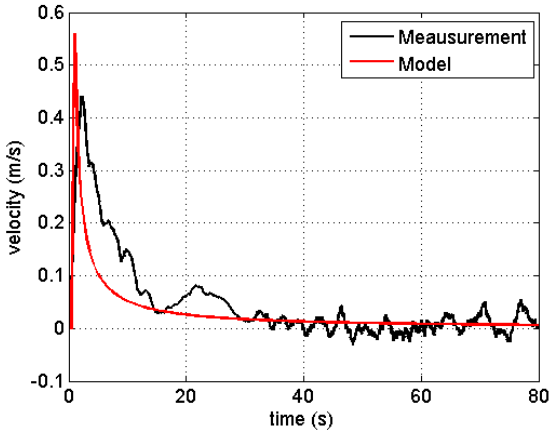

Figure 24. Vertical component of velocity in the bubble cloud 0.5 m above the airgun. Comparison between simplified model and measurement.

One can see from the figure that simulated water velocity reaches approximately the same value as measured but drops much faster. A reason for the slower drop of entrained water velocity in the measurements could be given as follows. Oscillations and break-up of the initial airgun bubble create many vortices in the water, which trap small bubbles. This slows down the rise of the bubbles. The vortices are not included into the model. Such an inclusion would be difficult even in CFD simulations unless they use the Large Eddy Simulation (LES) or the Direct Numerical Simulation (DNS) techniques, which are prohibitively time consuming even for this relatively simple geometry.

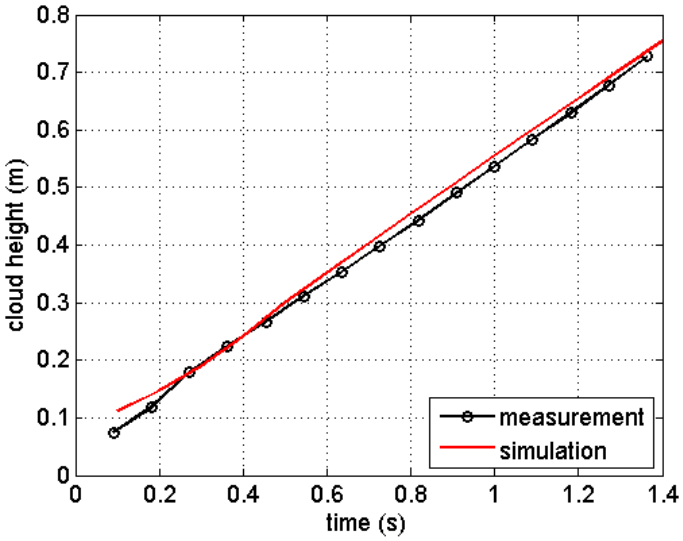

Figure 25. Time history of the top edge of the bubble cloud position above the airgun. Comparison of simulation with measurement.

Figure 25 compares the simulated time history of the top edge of the bubble cloud position above the airgun with the measurements using still images (Figure 5). Here we used the value of parameter $\beta = 0.8$ in equation (43).

The next step in developing model of the rising bubble cloud is to model the time history of the 'small' bubble fraction. We assume that small bubbles are initially uniformly distributed in a sphere of radius R_{c0} with the centre located at the final position, z_0, of the initial bubble before its break-up. The position of the centre, z_0 is the same as that of the bubble cloud of the 'large' bubble fraction. The radius of the cloud of the 'small' bubble fraction could be, however, different from that of the cloud of the 'large' bubble fraction: $R_{c0} = \alpha_s r_{c0}$, with $\alpha_s \geq 1$. For each bubble size and bubble initial position we find its rising trajectory by solving numerically the following kinematic equations:

$$\begin{aligned} \frac{dz_b}{dt} &= U_s(d_b) + u(z,r,t), \\ \frac{dr_b}{dt} &= v(z,r,t), \end{aligned} \tag{46}$$

with initial conditions:

$$z_b = z_{b0}, \qquad r_b = r_{b0} \;\; at \;\; t = 0. \tag{47}$$

Obviously, we assume in equation (46) that the velocity of a bubble relative to the water is equal to the bubble terminal velocity. We also neglect here the dependence of the terminal velocity on the bubble depth and calculate it at the initial bubble depth. From these bubble trajectories and the bubble size distribution in the initial bubble cloud, estimated from the model of bubble break-up, we can calculate the bubble size distribution at any point in the water and moment of time. For this, we first divide the initial bubble cloud into small volumes, $V_0 = \pi \Delta z_0((r_{b0} + \Delta r_0)^2 - (r_{b0} - \Delta r_0)^2)$. The number of bubbles of size d_b in the volume V_0 can be calculated as

$$n_{b0}(d_b, z_{b0}, r_{b0}) = \frac{n_b(d_b)V_0}{V_{bc}}, \tag{48}$$

where $V_{bc} = \frac{4\pi}{3} R_{c0}^3$ is the volume of the initial bubble cloud, and $(z_{b0} - z_0)^2 + r_{b0}^2 \leq R_{c0}^2$. $n_b(d_b)$ is the total number of bubbles of size d_b in the initial bubble cloud after the bubble break-up by turbulence.

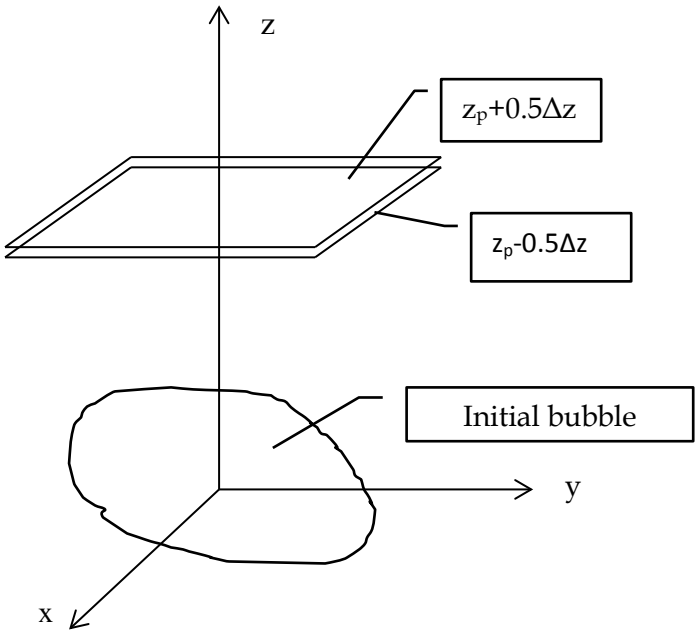

Figure 26. Geometry for calculating acoustic transmission through bubble cloud.

Once we know the bubble size distribution as a function of spatial coordinates and time, $n(d_b, z, r, t)$, we can calculate the acoustic transmission through the bubble cloud at a certain depth to compare it with the experiment (Figure 1). For this we need to calculate $n_p(d_b, r, t)$, the time history of the bubble size distribution per unit volume, averaged over the thickness Δz of a horizontal layer at height z_p above the airgun (Figure 26), at which the acoustic transmission through the bubble cloud was measured in the experiment (Figure 1). The absorption due to bubbles is calculated at the sound frequency f, as [10]

$$\alpha_b(r, t, f) = 4.34 S_e = 4.34 \sum_{i=1}^{N} \sigma_e(d_{bi}, f) n_p(d_{bi}, r, t), \tag{49}$$

where S_e is the extinction cross section per unit volume, and the extinction cross section of a single bubble

$$\sigma_e(d_{bi}, f) = \frac{\pi d_{bi}^2 (\delta/\delta_r)}{[(f_R/f)^2 - 1]^2 + \delta^2}, \tag{50}$$

where the total damping constant

$$\delta = \delta_r + \delta_t + \delta_v \tag{51}$$

is the sum of the reradiation term δ_r, the thermal damping term δ_t, and the viscous damping term δ_v. The damping terms and the resonance frequency, f_R, depend on the physical properties of the bubble gas and the ambient fluid as well as bubble depth. The corresponding equations are given in section 8.2 of [10] and we do not reproduce them here.

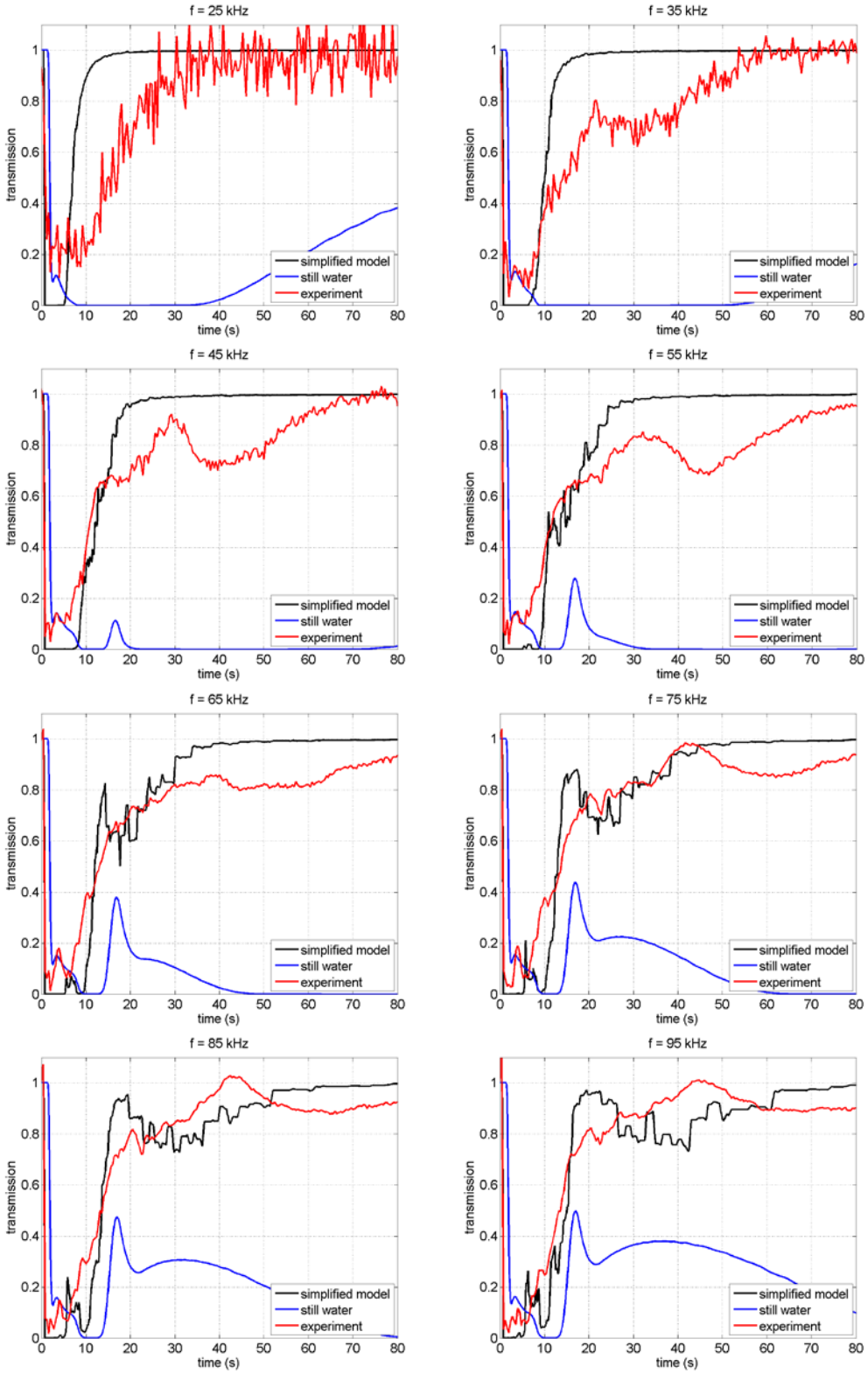

Figure 27. Time history of the transmission through the rising bubble cloud in various frequency bands.

Transmission through the bubble cloud can then be calculated as:

$$\tau(t,f) = \frac{A_t}{A_0} = \exp\left(-\frac{2}{8.68}\int_0^\infty \alpha_b(r,t,f)dr\right), \tag{52}$$

where A_t and A_0 are the amplitude of the signal received by the hydrophone with and without the bubble cloud, respectively. To compare the simulated results, which are calculated at a single frequency value, to the measurements taken using a frequency sweep pulse, we filter the transmitted signal into narrow frequency bands of 10 kHz using the 4-node Butterworth filter. The simulated results are then calculated at the centre frequency of each band. The comparison between simulated acoustic transmission through the rising bubble cloud with the measurement is presented in Figure 27. Here we also plot results obtained by the previous model where entrainment of the water was not taken into account. Although the model does not provide a perfect match with the experiment, the simulations using the simplified model of the water entrainment (black curves) compares significantly better with the measurement than the model of bubble rise in still water (blue curves).

5. Conclusion

A previously developed model of the remnant bubble cloud of underwater explosion has been improved by taking into account interaction between bubbles through water entrainment. In the new model, the bubbles in the cloud are divided into two fractions of large and small bubbles and a simplified model of water entrainment by the large bubble fraction has been developed. The dynamics of rising small bubbles is calculated in the assumption that their velocity is constant and is the sum of the terminal velocity in still water and that of the entrained water. The time history of the bubble size and spatial distribution in the cloud can then be easily computed. The calculation of acoustic properties of the bubble cloud is straightforward after that.

To validate the new model, an experiment was conducted in the acoustic tank of the Underwater Acoustic Scattering Laboratory. The underwater explosion was emulated by a small airgun. The model of the explosion bubble dynamics was modified to the parameters of the airgun demonstrating a fair agreement with measured time history of the oscillating bubble radius. The simplified model of the water entrainment was validated by comparison of the water velocity at the axis of the bubble cloud with the corresponding measurements using an acoustic Doppler velocimeter. Finally, a comparison was made between the simulated and measured acoustic transmission through the bubble cloud. Although a perfect agreement was not achieved, a significant improvement against the previous model was demonstrated.

6. References

1. Kouzoubov, A., et al., *Acoustic Model of the Remnant Bubble Cloud from Underwater Explosion*, in *Acoustics 2012*. 2012: Fremantle, Australia.
2. Kouzoubov, A. and S. Wood, *UNDEX bubble cloud model. Laboratory experiments in support of model development and validation*. 2014, DSTO.
3. de Graaf, K., *The Bubble Dynamics and Pressure Field Generated by a Seismic Airgun*, in *National Centre for Maritime Engineering and Hydrodynamics*. 2013, Australian Maritime College. University of Tasmania.
4. Harris, G., et al., *UNDEX Perturbation Test Program. Quick Look report*. 2010: Naval Undersea Warfare Center. Newport.
5. Tomiyama, A., et al., *Drag coefficients of single bubbles under normal and micro gravity conditions.* JSME International Journal, Series B (Fluids and Thermal Engineering), 1998. **41**(2): p. 472-479.
6. Kouzoubov, A., J. Castano, and C. Godoy, *Bubble Cloud Rise and Interaction with a Bubble Layer*. 2012, DSTO, NUWC.
7. Martinez Mercado, J., et al., *On bubble clustering and energy spectra in pseudo-turbulence.* Journal of Fluid Mechanics, 2010. **650**: p. 287-306.
8. Caruthers, J.W., et al., *An iterative approach for approximating bubble distributions from attenuation measurements.* Journal of the Acoustical Society of America, 1999. **106**(1): p. 185-189.
9. Commander, K.W. and R.J. McDonald, *Finite-element solution of the inverse problem in bubble swarm acoustics.* The Journal of the Acoustical Society of America, 1991. **89**(2): p. 592-597.
10. Medwin, H. and C. Clay, *Fundamentals of acoustical oceanography*. 1998, Sydney: Academic Press.
11. Geers, T.L. and K.S. Hunter, *An integrated wave-effects model for an underwater explosion bubble.* J. Acoust. Soc. Am., 2002. **111**(4): p. 1584-1601.
12. Hsiao, C.-T., G.L. Chahine, and L. Han-Lieh, *Scaling effect on prediction of cavitation inception in a line vortex flow.* Transactions of the ASME. Journal of Fluids Engineering, 2003. **125**(1): p. 53-60.
13. Brennen, C.E., *Fission of collapsing cavitation bubbles*. Journal of Fluid Mechanics, 2002. **472**: p. 153-166.
14. Cole, R.H., *Underwater Explosions*. 1948, Princeton: Princeton University Press.
15. Wilcox, D.C., *Turbulence Modeling for CFD*. 1994, La Canada CA: DCW Industries, Inc.
16. Lasheras, J.C., et al., *A review of statistical models for the break-up of an immiscible fluid immersed into a fully developed turbulent flow.* International Journal of Multiphase Flow, 2002. **28**: p. 247-278.
17. Martínez-Bazán, C., J.L. Montañés, and J.C. Lasheras, *On the breakup of an air bubble injected into a fully developed turbulent flow. Part 1. Breakup frequency.* Journal of Fluid Mechanics, 1999. **401**: p. 157-182.
18. Martínez-Bazán, C., J.L. Montañés, and J.C. Lasheras, *On the breakup of an air bubble injected into a fully developed turbulent flow. Part 2. Size PDF of the resulting daughter bubbles.* Journal of Fluid Mechanics, 1999. **401**: p. 183-207.
19. *ANSYS CFX-Solver, Release 13.0: Theory*. 2010.

DEFENCE SCIENCE AND TECHNOLOGY GROUP DOCUMENT CONTROL DATA			1. DLM/CAVEAT (OF DOCUMENT)
2. TITLE Bubble Cloud Generation by an Airgun: Laboratory experiments and modelling		3. SECURITY CLASSIFICATION (FOR UNCLASSIFIED LIMITED RELEASE USE (U/L) NEXT TO DOCUMENT CLASSIFICATION) Document (U) Title (U) Abstract (U)	
4. AUTHOR(S) Alexei Kouzoubov and Shane Wood		5. CORPORATE AUTHOR Defence Science and Technology Group PO Box 1500 Edinburgh SA 5111	
6a. DST GROUP NUMBER DST-Group-TR-3379	6b. AR NUMBER AR-016-902	6c. TYPE OF REPORT Technical Report	7. DOCUMENT DATE July 2017
8. OBJECTIVE ID AV14990161	9.TASK NUMBER 07/333	10.TASK SPONSOR CASG	
11. MSTC Undersea Command and Control		12. STC Underwater Weapons Systems	
13. DOWNGRADING/DELIMITING INSTRUCTIONS		14. RELEASE AUTHORITY Chief, Maritime Division	
15. SECONDARY RELEASE STATEMENT OF THIS DOCUMENT *Approved for public release* OVERSEAS ENQUIRIES OUTSIDE STATED LIMITATIONS SHOULD BE REFERRED THROUGH DOCUMENT EXCHANGE, PO BOX 1500, EDINBURGH, SA 5111			
16. DELIBERATE ANNOUNCEMENT No Limitations			
17. CITATION IN OTHER DOCUMENTS Yes			
18. RESEARCH LIBRARY THESAURUS Wakes, Underwater Explosions, Bubbles, Acoustic measurement			
19. ABSTRACT Laboratory experiments in support of the development and validation of a model of bubble cloud resulting from an underwater explosion are described in this report. The underwater explosion was emulated by a small airgun. The elements of the model are presented in detail. Special attention is paid to the model improvements with respect to accounting for bubble interaction in the rising bubble cloud through water entrainment. Model results are compared to the experimental measurements and high-fidelity numerical simulations.			